Appendix A

Probability Theory

Probability theory is essential to statistical physics. This is because when we look at a macroscopic system (e.g., a balloon filled with air) we do not know precisely the microscopic state of the system (i.e., the positions and momenta of all its molecules). This appendix provides the essential concepts of probability theory that are needed in this book.

If we, for instance, throw a dice we have 6 different possible outcomes, each of which occurs with a probability $1/6$. In more general terms, one has a set of possible events E_i, $i = 1, \ldots, n$ ($n = 6$ for a dice) and each event has a certain probability $p_i = p(E_i)$ with $0 \leq p(E_i) \leq 1$. The sum of the probabilities must add up to 1 (since one of all possible events has to occur), i.e.,

$$\sum_{i=1}^{N} p_i = 1. \tag{A.1}$$

It is also possible that the outcome is continuous, e.g., the orientation of a wheel of fortune with respect to some reference direction can obtain an angle α between $-\pi$ and π. In that case $p(\alpha)$ is a function defined on the interval $-\pi \leq \alpha \leq \pi$, called the probability distribution. As in the discrete case one has $\int_{-\pi}^{\pi} p(\alpha)\, d\alpha = 1$ or in more general terms

$$\int p(x)\, dx = 1 \tag{A.2}$$

where the integral has to be taken over the allowed values of the continuous variable x (or, alternatively, one can set $\rho(x) = 0$ if x

cannot occur and the integral can then be taken from $-\infty$ to $+\infty$). If the wheel is perfect then $\rho(\alpha)$ is constant in the relevant interval of angles. It then follows from Eq. A.2 that $\rho(\alpha) = 1/(2\pi)$ for all $-\pi \leq \alpha \leq \pi$.

A random variable (or stochastic variable) is a function f that attributes to each possible outcome (discrete or continuous) a number. For instance, for the case of a dice, we could choose the function $f_i = i$ that attributes to each outcome the number of eyes. We can then define the expectation value of such a variable as follows

$$\langle f \rangle = \sum_{i=1}^{N} f_i \, p_i. \tag{A.3}$$

Let us consider the case of a dice for two different stochastic variables. For $f_i = i$ one finds $\langle f \rangle = 7/2$ and for $f_i = 1$ one finds $\langle f \rangle = 1$. The expectation value for a continuous variable can be defined in a similar way, namely

$$\langle f \rangle = \int f(x) \, p(x) \, dx. \tag{A.4}$$

The special case $\langle x \rangle$ is called the average of the distribution. For the above named example of a wheel of fortune and choosing $f(\alpha) = \alpha$ we find $\langle \alpha \rangle = 0$. More generally, $\mu_m = \langle x^m \rangle$ is called the m-th moment of the distribution.

Of particular importance is the standard deviation σ_f of f or its square, σ_f^2, the variance. It is defined by

$$\sigma_f^2 = \left\langle (f - \langle f \rangle)^2 \right\rangle. \tag{A.5}$$

One squares here the quantity $f - \langle f \rangle$ since otherwise this expression would average out to zero, $\langle f - \langle f \rangle \rangle \equiv 0$. σ_f is a measure of how much the stochastic variable varies around the mean value when one repeats the experiment (throwing the dice, turning the wheel, etc.) over and over again. One can rewrite σ_f^2 as follows $\left\langle (f - \langle f \rangle)^2 \right\rangle = \left\langle f^2 - 2 f \langle f \rangle + \langle f \rangle^2 \right\rangle = \left\langle f^2 \right\rangle - \langle f \rangle^2$, i.e.,

$$\sigma_f^2 = \left\langle f^2 \right\rangle - \langle f \rangle^2. \tag{A.6}$$

For example, for a dice and $f_i = i$ we find $\sigma_f^2 = 91/6 - 49/4 = 35/12$. The typical deviation σ_f from the mean value is thus about 1.7.

The most important of all the probability distributions is the Gaussian distribution that we shall encounter many times in this book. It is of the form $\rho(x) \sim e^{-(x-\mu)^2/(2\sigma^2)}$ where μ and σ are some arbitrary numbers. This distribution needs to be normalized to one, see Eq. A.2. This is easy if you know that

$$\int_{-\infty}^{\infty} e^{-x^2} dx = \sqrt{\pi}. \tag{A.7}$$

This integral is worthwhile remembering by heart. Hence

$$\int_{-\infty}^{\infty} e^{-(x-\mu)^2/(2\sigma^2)} dx = \sqrt{2\pi}\sigma. \tag{A.8}$$

This means that the Gaussian distribution is normalized to one if we choose

$$\rho(x) = \frac{1}{\sqrt{2\pi}\sigma} e^{-(x-\mu)^2/(2\sigma^2)}. \tag{A.9}$$

This distribution is depicted in Fig. A.1. Let us calculate now the average $\langle x \rangle$ and the variance $\langle x^2 \rangle - \langle x \rangle^2$ of this distribution. We start with the average:

$$\langle x \rangle = \frac{1}{\sqrt{2\pi}\sigma} \int_{-\infty}^{\infty} x e^{-(x-\mu)^2/(2\sigma^2)} dx = \frac{1}{\sqrt{2\pi}\sigma} \times \int_{-\infty}^{\infty} (u+\mu) e^{-u^2/(2\sigma^2)} du = \mu. \tag{A.10}$$

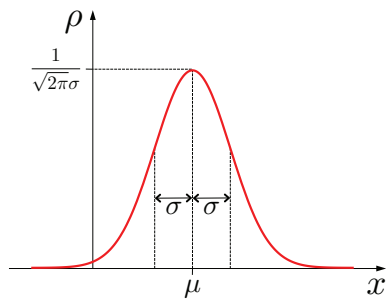

Figure A.1 The Gaussian distribution.

For the last step we use the fact that the integral over $ue^{-u^2/(2\sigma^2)}$ vanishes since this is an odd function, i.e., a function with the symmetry $f(-u) = -f(u)$. The remaining term gives simply μ since the Gaussian distribution is normalized.

Next we calculate the variance of the Gaussian distribution:

$$\begin{aligned}\left\langle (x-\mu)^2 \right\rangle &= \frac{1}{\sqrt{2\pi}\sigma} \int_{-\infty}^{\infty} (x-\mu)^2 \, e^{-(x-\mu)^2/(2\sigma^2)} dx \\ &= -2\sigma^2 \left. \frac{d}{da} \right|_{a=1} \frac{1}{\sqrt{2\pi}\sigma} \int_{-\infty}^{\infty} e^{-a(x-\mu)^2/(2\sigma^2)} dx \end{aligned} \tag{A.11}$$

Here we introduced a new help variable a. Taking the derivate of the exponential with respect to a and then setting a to one gives us just the factor $(x-\mu)^2$ we need. Using Eq. A.8 gives then

$$\left\langle (x-\mu)^2 \right\rangle = -\sqrt{\frac{2}{\pi}}\sigma \left. \frac{d}{da} \right|_{a=1} \sqrt{\frac{2\pi}{a}}\sigma = \sigma^2. \tag{A.12}$$

Hence μ and σ in the Gaussian distribution A.9 correspond to its average and standard deviation.

The Gaussian distribution can be defined for a set of random variables $x_1, x_2, \ldots, x_N$ as

$$\rho(x_1, x_2, \ldots, x_N) = C \exp\left(-\frac{1}{2} \sum_{n,m=1}^{N} A_{nm} (x_n - B_n)(x_m - B_m) \right) \tag{A.13}$$

where C is a normalization constant and A_{nm} is a symmetric positive definite matrix, i.e., $A_{nm} = A_{mn}$ and $\sum_{m,n} A_{nm} x_n x_m \geq 0$ for all x_n. Through the coordinate transformation $y_n = x_n - B_n$ the distribution, Eq. A.13, takes the form

$$\rho(y_1, y_2, \ldots, y_N) = C \exp\left(-\frac{1}{2} \sum_{n,m=1}^{N} A_{nm} y_n y_m \right). \tag{A.14}$$

Higher moments of such a multivariate Gaussian distribution with zero mean have remarkable properties. Whereas odd moment like $\langle y_i y_j y_k \rangle$ vanish due to the symmetry of the distribution, even moments can be broken down into sums over products of second moments. Without proof we give here the general formula:

$$\left\langle y_{n_1} y_{n_2} \ldots y_{n_{2p}} \right\rangle = \sum_{\text{all pairings}} \left\langle y_{m_1} y_{m_2} \right\rangle \left\langle y_{m_3} y_{m_4} \right\rangle \ldots \left\langle y_{m_{2p-1}} y_{m_{2p}} \right\rangle. \tag{A.15}$$

The set of subscripts $\{m_1, m_2, \ldots, m_{2p}\}$ stands for the permutation of the original set $\{n_1, n_2, \ldots, n_{2p}\}$. The summation is taken over all possible pairings. To give a concrete example, we present the fourth moment:

$$\langle y_n y_m y_k y_l \rangle = \langle y_n y_m \rangle \langle y_k y_l \rangle + \langle y_n y_k \rangle \langle y_m y_l \rangle + \langle y_n y_l \rangle \langle y_m y_k \rangle . \quad \text{(A.16)}$$

Another important property of the Gaussian distribution, Eq. A.14, is that any linear combination of the y_n's, e.g., an expression of the form

$$Y = \sum_{n=1}^{N} a_n y_n \quad \text{(A.17)}$$

is again Gaussian distributed. Specifically one has

$$\rho(Y) = \frac{1}{\sqrt{2\pi \langle Y^2 \rangle}} \exp\left(-\frac{Y^2}{2\langle Y^2 \rangle}\right) \quad \text{(A.18)}$$

with $\langle Y^2 \rangle = \sum_{n,m} a_n a_m \langle y_n y_m \rangle$. This can be shown as follows. One obtains $\rho(Y)$ by picking out all those states that fulfill Eq. A.17:

$$\rho(Y) = \int \rho(y_1, y_2, \ldots, y_N)\, \delta\left(Y - \sum_{n=1}^{N} a_n y_n\right) dy_1 \ldots dy_N. \quad \text{(A.19)}$$

Let us first integrate over y_1. What is then left is an $(N-1)$-dimensional integral over the remaining variables y_2 to y_N. The integrand is the Gaussian distribution, Eq. A.14, but with y_1 replaced by $a_1^{-1}\left(Y - \sum_{n\neq 1} a_n y_n\right)$. This integrand is again a Gaussian function of $y_2, y_3, \ldots, y_N$ and Y. For each of those variables the integrand is of the form $\exp\left(-ay^2 + by\right)$ where y stands for the variable and a and b are complicated expressions. a is a combination of the constant coefficients a_i and A_{ij} and is thus also some constant. b is a linear combination of the other remaining variables. Luckily we do not need to calculate these terms explicitly. All we need to know is that when we successively integrate over the y_i's we always find a Gaussian function in the remaining variables since

$$\int_{-\infty}^{\infty} e^{-ay^2 - by} dy = e^{\frac{b^2}{4a}} \int_{-\infty}^{\infty} e^{-a\left(y + \frac{b}{2a}\right)^2} dy = \sqrt{\frac{\pi}{a}} e^{\frac{b^2}{4a}}. \quad \text{(A.20)}$$

Thus, after having integrated over all N y_i's we remain with a Gaussian distribution in Y. Since its average vanishes, we know that it must be of the form given in Eq. A.18.

Appendix B

The Distribution of Magnetization and the Central Limit Theorem

We derive here explicitly an approximation for the number of microstates of the system shown in Fig. 2.6 for a given value M of the magnetization. The distribution that we shall find follows also via the central limit theorem that we discuss further below in this appendix.

Let us give an approximate expression for the number of microstates to a given macrostate, Eq. 2.47. We consider deviations from the most probable state $k = N/2$, namely $k = \frac{N}{2} + m$. This corresponds to a magnetization $M = 2\mu m$. We assume $m \ll N$ that allows us to use Stirling's formula, Eq. 2.48:

$$N_{\text{micro}}(M) = \binom{N}{\frac{N}{2}+m} \approx \frac{N^{N+\frac{1}{2}}}{\sqrt{2\pi}\left(\frac{N}{2}+m\right)^{\frac{N}{2}+m+\frac{1}{2}}\left(\frac{N}{2}-m\right)^{\frac{N}{2}-m+\frac{1}{2}}}$$
$$= \frac{N_{\max}}{\left(1-4m^2/N^2\right)^{\frac{N+1}{2}}}\left(\frac{1-\frac{2m}{N}}{1+\frac{2m}{N}}\right)^m \tag{B.1}$$

with $N_{\max}$ given by Eq. 2.49. Approximating the exponent $(N+1)/2$ by $N/2$ and dropping for the second factor terms of the order $m(m/N)^2$ we obtain

$$N_{\text{micro}}(M) \approx \frac{N_{\max}}{\left(1-4m^2/N^2\right)^{N/2}}\left(1-\frac{4m^2}{N}\right). \tag{B.2}$$

The denominator in Eq. B.2 can be approximated by an exponential function since

$$\left(1+\frac{x}{K}\right)^{K} \overset{K\to\infty}{\to} e^{x} \tag{B.3}$$

here with $K = N/2$. Furthermore, we use the fact that $1 - 4m^2/N$ is the beginning of the power series of the exponential function $\exp\left(-4m^2/N\right)$. We can thus approximate

$$N_{\text{micro}}(M) \approx \frac{N_{\max}}{e^{-2m^2/N}} e^{-4m^2/N} = N_{\max} e^{-2m^2/N}. \tag{B.4}$$

Replacing m in Eq. B.4 by $M/2\mu$ we arrive at Eq. 2.50.

Instead of doing this explicitly by expanding Eq. B.1 using Stirling's formula that—as we just saw—is quite cumbersome, one can make use of the famous central limit theorem. It states that the sum of a sufficiently large number of independent and identically distributed random variables X_i with a finite mean μ and standard deviation σ is Gaussian distributed. In other words if we introduce the sum

$$X = \sum_{i=1}^{N} X_i \tag{B.5}$$

then for sufficiently large N one finds

$$\rho(X) = \frac{1}{\sqrt{2\pi N}\sigma} e^{-\frac{(X-N\mu)^2}{2N\sigma^2}} \tag{B.6}$$

irrespective of the shape of the distribution of the individual variables X_i. We give this here without proof but as a consistency check we calculate

$$\sigma_X^2 = \left\langle X^2 \right\rangle - \langle X \rangle^2 = \sum_{i,j=1}^{N} \left\langle X_i X_j \right\rangle - \sum_{i,j=1}^{N} \langle X_i \rangle \left\langle X_j \right\rangle. \tag{B.7}$$

Since the random variables are independent from each other, one has $\left\langle X_i X_j \right\rangle = \langle X_i \rangle \left\langle X_j \right\rangle$ for all $i \neq j$. What remains are all the diagonal terms $i = j$ leading to

$$\sigma_X^2 = \sum_{i=1}^{N} \left\langle X_i^2 \right\rangle - \sum_{i=1}^{N} \langle X_i \rangle^2 = \sum_{i=1}^{N} \sigma^2 = N\sigma^2. \tag{B.8}$$

This is indeed the variance of the distribution given in Eq. B.6.

If we use for X the magnetization that is the sum of the individual magnetic moments μs_i with $\langle \mu s_i \rangle = 0$ and $\sigma = \mu$, we find immediately from Eq. B.6 that $\rho(M) \sim e^{-\frac{M^2}{2N\mu^2}}$ which leads directly to Eq. 2.50.

Appendix C

Hamilton's Principle and the Pendulum

Consider a particle of mass M in one dimension. Its position at time t is given by $x(t)$. Assume that the particle feels a time-dependent force $f(t)$. Newton's second law states that the particle's mass times its acceleration, $\ddot{x}(t) = d^2x(t)/dt^2$, equals that force:

$$M\ddot{x}(t) = f(t). \tag{C.1}$$

This so-called equation of motion is solved straightforwardly:

$$x(t) = x_0 + v_0 t + \frac{1}{M}\int_0^t dt' \int_0^{t'} dt'' f\left(t''\right) \tag{C.2}$$

with $x(0) = x_0$ and $\dot{x}(0) = v_0$ denoting the initial position and velocity of the particle. As a special case of Eq. C.1 consider a particle in an external potential $V(x)$. In that case $f(t) = -dV(x(t))/dx$ and hence

$$M\ddot{x}(t) = -\frac{dV(x(t))}{dx}. \tag{C.3}$$

We introduce now Hamilton's principle which states that the dynamics of such a physical system is determined by a variational principle. As the first step we write down the Lagrange function L of the system that is given by the kinetic minus the potential energy. For the particle in the potential this leads to

$$L(x(t), \dot{x}(t)) = \frac{1}{2}M\dot{x}^2(t) - V(x(t))$$

Next we introduce the so-called action functional

$$S[x] = \int_0^T L(x(t), \dot{x}(t))\, dt. \tag{C.5}$$

A functional maps a function, here $x(t)$, onto a number, here $S[x]$. The square brackets indicate that the argument is not a number but an entire function.

Hamilton's principle states that the time evolution of the system, $x(t)$, corresponds to a stationary point of the action, Eq. C.5. More precisely, of all the curves $x(t)$ with given start point $x(0) = x_0$ and given end point $x(T) = x_T$ the true solution is the one that is a minimum or a saddle point (in short a stationary point) of the action. We need now to define the meaning of a stationary point for a functional more precisely. We consider a small perturbation $h(t)$ around a given function $x(t)$. The new function $x(t) + h(t)$ needs to have the same start and end points, i.e., we require $h(0) = h(T) = 0$. Now let us consider

$$S[x+h] = \int_0^T L\left(x(t) + h(t), \dot{x}(t) + \dot{h}(t)\right) dt. \tag{C.6}$$

A Taylor expansion of the Lagrange function to first order leads to

$$S[x+h] = S[x] + \int_0^T \left(\frac{\partial L}{\partial x} h + \frac{\partial L}{\partial \dot{x}} \dot{h}\right) dt + O\left(\|h\|^2\right) \tag{C.7}$$

where $O(\|h\|^2)$ stands for higher order terms, namely integrals that contain terms like $h^2(t)$ and $\dot{h}^2(t)$. Through integration by parts, namely replacing $\dot{h}\partial L/\partial \dot{x}$ by $\frac{d}{dt}(h\partial L/\partial \dot{x}) - h\frac{d}{dt}(\partial L/\partial \dot{x})$ and using the fact that the boundary terms vanish, one arrives at

$$S[x+h] - S[x] = \int_0^T \left(\frac{\partial L}{\partial x} - \frac{d}{dt}\frac{\partial L}{\partial \dot{x}}\right) h\, dt + O\left(\|h\|^2\right). \tag{C.8}$$

One says that $x(t)$ is a stationary point of S if the integral vanishes for any small h. This is the case if $x(t)$ fulfills the so-called Euler–Lagrange equation

$$\frac{\partial L}{\partial x} - \frac{d}{dt}\frac{\partial L}{\partial \dot{x}} = 0. \tag{C.9}$$

Let us take the Lagrange function from above, Eq. C.4, as an example. By inserting it into the Euler–Lagrange equation, Eq. C.9, we find the equation of motion, Eq. C.3. For this special case we can thus indeed verify that the time evolution of the system, the solution of Eq. C.3, is a stationary point of the action, Eq. C.5. It is straightforward to extend the formalism to d dimensions where one obtains d Euler–Lagrange equations, one for each direction in space. One can then easily verify that this set of equations is identical to the equations of motion for a particle in d dimensions.

So far it looks like Hamilton's principle is a very complicated way of obtaining the equation of motion, Eq. C.3, that one can write down immediately. For more complicated systems that contain certain constraints, however, such a framework is extremely useful. To give an example consider the pendulum depicted on the rhs of Fig. 4.20. It consists of a mass M attached to a massless rod of length l that is suspended from a pivot at position $(x, y) = (0, 0)$ around which it can swing freely. The potential of the mass in the gravitational field is given by Mgy. The Lagrange function of the pendulum is thus given by

$$L(x, y, \dot{x}, \dot{y}) = \frac{M}{2}\left(\dot{x}^2 + \dot{y}^2\right) - Mgy. \tag{C.10}$$

The Euler–Lagrange equations for the X- and Y-coordinates lead to two equations of motion, $\ddot{x} = 0$ and $\ddot{y} = -g$.

Unfortunately these equations are completely wrong. Why? What we found are the equations of motion of a free particle in 2 dimensions in a gravitational field. Solutions are e.g., trajectories of rain drops or of cannon balls but certainly not the motion of a pendulum. What went wrong? We forgot to take into account the presence of the rod that imposes the constraint $x^2 + y^2 = l^2$. A better approach would be to use a coordinate system that accounts automatically for this constraint, namely to describe the state of the pendulum by the angle $\theta(t)$ between the pendulum and the Y-direction, see Fig. 4.20. But how does the equation of motion look like in terms of this angle?

Here comes into play a great advantage of Hamilton's principle: it is independent of the coordinate system that one chooses. Suppose one goes from one coordinate system $x_1, x_2, \ldots, x_N$ to another coordinate system $q_1, q_2, \ldots, q_f$ via the transformations $\mathbf{q} = \mathbf{q}(\mathbf{x})$

and $\mathbf{x} = \mathbf{x}(\mathbf{q})$. The trajectory $\mathbf{x}(t)$ becomes then $\mathbf{q}(\mathbf{x}(t))$. The action functional can then be rewritten as

$$S[\mathbf{x}] = \int_0^T L(\mathbf{x}(t), \dot{\mathbf{x}}(t))\, dt = \int_0^T L\left(\mathbf{x}(\mathbf{q}(t)), \sum_{i=1}^{f} \frac{\partial \mathbf{x}(\mathbf{q}(t))}{\partial q_i} \dot{q}_i\right) dt. \tag{C.11}$$

The rhs of Eq. C.11 is again of the form

$$S[\mathbf{q}] = \int_0^T \tilde{L}(\mathbf{q}(t), \dot{\mathbf{q}}(t))\, dt \tag{C.12}$$

with a new Lagrange function $\tilde{L}$. Also here Hamilton's principle must hold, i.e., the dynamic evolution of the system follows from the Euler–Lagrange equations

$$\frac{\partial \tilde{L}}{\partial q_i} - \frac{d}{dt}\frac{\partial \tilde{L}}{\partial \dot{q}_i} = 0 \tag{C.13}$$

for $i = 1, \ldots, f$.

If we have a system with constraints we can sometimes introduce coordinates that automatically fulfill those constraints. The equations of motion are then simply given by the Euler–Lagrange equations in these coordinates. Let us go back to the pendulum. We describe now the configuration of the pendulum by the angle $\theta(t)$ that measures the deviation from the vertically upwards pointing position, see Fig. 4.20. In terms of this angle the kinetic energy of the pendulum is given by $Ml^2\dot{\theta}^2/2$ and the potential energy by $Mlg\cos\theta$. This leads to the following Lagrange function:

$$L(\theta, \dot{\theta}) = \frac{Ml^2}{2}\dot{\theta}^2 - Mgl\cos\theta. \tag{C.14}$$

The corresponding Euler–Lagrange equation is given by

$$\ddot{\theta}(t) = \frac{g}{l}\sin\theta(t). \tag{C.15}$$

We have thus found the equation of motion of the pendulum. In the following we solve this equation that—as we shall see—is rather cumbersome. We present this calculation here since it leads to the explicit formulas on which the plots of the Euler elasticas in Fig. 4.22 are based. We start by multiplying Eq. C.15 on both sites with $2\dot{\theta}(t)$. This leads to

$$2\dot{\theta}(t)\ddot{\theta}(t) = \frac{2g}{l}\dot{\theta}(t)\sin\theta(t). \tag{C.16}$$

This is straightforward to integrate:

$$\dot{\theta}^2(t) = -\frac{2g}{l}\cos\theta(t) + C \tag{C.17}$$

with C being an integration constant. By multiplying this equation on both sides with $Ml^2/2$ the physical meaning of C becomes obvious:

$$\frac{Ml^2}{2}\dot{\theta}^2(t) + Mgl\cos\theta(t) = \frac{Ml^2}{2}C = E_{\text{tot}} - Mgl. \tag{C.18}$$

We introduce here E_{tot}, the total energy of the pendulum, with its zero energy chosen to correspond to the resting state of the pendulum, $\theta(t) \equiv \pi$. Thus the integration constant C reflects the total energy that is a conserved quantity: the sum of the kinetic and potential energy is always constant. Using the identity $\cos\theta = 1 - 2\sin^2(\theta/2)$ we can rewrite Eq. C.18 as follows:

$$\frac{\dot{\theta}^2(t)}{4} = \frac{1}{2Ml^2}\left(E_{\text{tot}} - 2Mlg + 2Mlg\sin^2\left(\frac{\theta(t)}{2}\right)\right). \tag{C.19}$$

Taking the square-root we obtain

$$\frac{\dot{\theta}(t)}{2} = \pm\sqrt{\frac{g}{l}}\sqrt{\frac{E_{\text{tot}}}{2Mlg} - 1 + \sin^2\left(\frac{\theta(t)}{2}\right)}. \tag{C.20}$$

It is convenient to rewrite Eq. C.20 in terms of the angle $\alpha = \pi - \theta$ that gives the deviation from the resting position. With $\sin^2(\theta/2) = 1 - \sin^2(\alpha/2)$ we obtain

$$\begin{aligned}\frac{\dot{\theta}(t)}{2} = -\frac{\dot{\alpha}(t)}{2} &= \pm\sqrt{\frac{g}{l}}\sqrt{\frac{E_{\text{tot}}}{2Mlg} - \sin^2\left(\frac{\alpha(t)}{2}\right)} \\ &= \pm\sqrt{\frac{g}{lm}}\sqrt{1 - m\sin^2\left(\frac{\alpha(t)}{2}\right)}\end{aligned} \tag{C.21}$$

where we introduced

$$m = \frac{2Mlg}{E_{\text{tot}}}. \tag{C.22}$$

Note that $2Mlg$ is the difference in potential energy between the topmost position, $\alpha = \pi$, and the lowest one, $\alpha = 0$. When $m > 1$ the total energy is smaller than the range of possible potential energies. This means that the pendulum cannot reach $\alpha = \pi$ and instead oscillates back and forth around the $\alpha = 0$ position. On the other

hand, for $0 < m < 1$ the total energy exceeds $2Mlg$. In that case the pendulum has still kinetic energy when it reaches the top, $\alpha = \pi$. This corresponds to a revolving pendulum. The special case $m = 1$ is solved and discussed in the main text.

Separation of variables in Eq. C.21—using $\dot{\alpha} = d\alpha/dt$—leads to

$$\frac{d\alpha/2}{\sqrt{1 - m\sin^2\left(\frac{\alpha}{2}\right)}} = \mp\sqrt{\frac{g}{lm}}dt. \tag{C.23}$$

Depending on the case—oscillating or revolving—we need to consider different initial conditions. We start with the revolving case, $0 < m < 1$ for which we assume that at zero time the pendulum is pointing downwards, i.e., $\alpha(0) = 0$. We now integrate Eq. C.23 from the time $t' = 0$ with the angle $\alpha' = \alpha(0) = 0$ to some arbitrary time $t' = t$ with $\alpha' = \alpha(t)$:

$$\mp\sqrt{\frac{g}{lm}}t = \int_0^{\alpha(t)/2} \frac{d\alpha'/2}{\sqrt{1 - m\sin^2\left(\frac{\alpha'}{2}\right)}} = F\left(\frac{\alpha(t)}{2}\middle| m\right). \tag{C.24}$$

The integral on the rhs is called the elliptic integral of the first kind. We have thus now an expression for t as a function of α, $t = t(\alpha)$. We would like to invert this formula to obtain $\alpha = \alpha(t)$. The inverse of F is called the amplitude, i.e., $\mathrm{am}(x|m) = F^{-1}(x|m)$. Hence

$$\frac{\alpha(t)}{2} = \mathrm{am}\left(\mp\sqrt{\frac{g}{lm}}t\middle| m\right). \tag{C.25}$$

Taking the sin-function on both sides of Eq. C.25 we introduce yet another special function:

$$\sin\left(\frac{\alpha(t)}{2}\right) = \mathrm{sn}\left(\mp\sqrt{\frac{g}{lm}}t\middle| m\right) = -\mathrm{sn}\left(\pm\sqrt{\frac{g}{lm}}t\middle| m\right). \tag{C.26}$$

The function $\mathrm{sn}(x|m) = \sin(\mathrm{am}(x|m))$ is one of the so-called Jacobian elliptic functions. On the rhs of Eq. C.26 we used the fact that $\mathrm{sn}(-x|m) = -\mathrm{sn}(x|m)$. The identities $\cos\alpha = 1 - 2\sin^2(\alpha/2)$ and $\cos\alpha = -\cos\theta$ allow to rewrite Eq. C.26 in the form

$$\cos\theta(t) = 2\mathrm{sn}^2\left(\sqrt{\frac{g}{lm}}t\middle| m\right) - 1 \tag{C.27}$$

We have thus succeeded to solve the equation of motion for the revolving pendulum.

Next we study the oscillating pendulum, $m > 1$. We choose the time such that for $t = 0$ the pendulum has reached its maximal amplitude and thus $\dot{\alpha}(0) = 0$. We call the time for one complete cycle T_P, the period. Hence we have $\alpha(T_\mathrm{P}/4) = 0$. Now we have to integrate Eq. C.23 from the time $t' = T_\mathrm{P}/4$ with the angle $\alpha' = \alpha(T_\mathrm{P}/4) = 0$ to some arbitrary time $t' = t$ with $\alpha' = \alpha(t)$:

$$\mp\sqrt{\frac{g}{lm}}\left(t - \frac{T_\mathrm{P}}{4}\right) = \int_{\alpha(T_\mathrm{P}/4)/2}^{\alpha(t)/2} \frac{d\alpha'/2}{\sqrt{1 - m\sin^2\left(\frac{\alpha'}{2}\right)}} = F\left(\frac{\alpha(t)}{2}\middle| m\right). \tag{C.28}$$

Along similar lines as in Eqs. C.24 to C.27 we can invert this formula leading us to the solution for the oscillating pendulum:

$$\cos\theta(t) = 2\mathrm{sn}^2\left(\sqrt{\frac{g}{lm}}\left(t - \frac{T_\mathrm{P}}{4}\right)\middle| m\right) - 1. \tag{C.29}$$

We can simplify things a bit by introducing a shift in time by $T_\mathrm{P}/4$ resulting in

$$\cos\theta(t) = 2\mathrm{sn}^2\left(\sqrt{\frac{g}{lm}}t\middle| m\right) - 1. \tag{C.30}$$

Using the Kirchhoff kinetic analogy we can now write down the solutions for the Euler elasticas. Replacing $\sqrt{g/l}$ by $\sqrt{f/A} = 1/\lambda$ and t by s we can rewrite the revolving case, Eq. C.27, as follows:

$$\cos\theta(s) = 2\mathrm{sn}^2\left(\frac{1}{\sqrt{m}}\frac{s}{\lambda}\middle| m\right) - 1. \tag{C.31}$$

To make the parametric plots of Fig. 4.22 in Cartesian coordinates we need to perform the integrations:

$$(x(s), y(s)) = \left(\int_0^s \sin\theta(s')\,ds', \int_0^s \cos\theta(s')\,ds'\right). \tag{C.32}$$

We know already $\cos\theta(s)$ from which we obtain $\sin\theta(s) = \sqrt{1 - \cos^2\theta(s)}$:

$$\begin{aligned}\sin\theta(s) &= 2\mathrm{sn}\left(\frac{1}{\sqrt{m}}\frac{s}{\lambda}\middle| m\right)\sqrt{1 - \mathrm{sn}^2\left(\frac{1}{\sqrt{m}}\frac{s}{\lambda}\middle| m\right)} \\ &= 2\mathrm{sn}\left(\frac{1}{\sqrt{m}}\frac{s}{\lambda}\middle| m\right)\mathrm{cn}\left(\frac{1}{\sqrt{m}}\frac{s}{\lambda}\middle| m\right)\end{aligned} \tag{C.33}$$

introducing cn, another Jacobian elliptic function. Integrating this leads to yet another Jacobian elliptic function, $\mathrm{dn} = \sqrt{1 - m\mathrm{sn}^2}$:

$$x(s) = \frac{2\lambda}{\sqrt{m}}\left(1 - \mathrm{dn}\left(\frac{1}{\sqrt{m}}\frac{s}{\lambda}\middle| m\right)\right). \tag{C.34}$$

On the other hand, the integration over $\cos\theta(s)$ yields:

$$y(s) = \left(\frac{2}{m} - 1\right)s - \frac{2\lambda}{\sqrt{m}}E\left(\mathrm{am}\left(\frac{1}{\sqrt{m}}\frac{s}{\lambda}\middle| m\right)\middle| m\right) \tag{C.35}$$

with E denoting the elliptic integral of the second kind.

We discuss finally the Euler elasticas corresponding to the oscillating case, $m > 1$. The Kirchhoff analogy leads to

$$\cos\theta(s) = 2\mathrm{sn}^2\left(\frac{1}{\sqrt{m}}\frac{s}{\lambda}\middle| m\right) - 1 = 2\mathrm{sn}^2\left(\sqrt{m'}\frac{s}{\lambda}\middle| \frac{1}{m'}\right) - 1, \tag{C.36}$$

where we introduced the reciprocal parameter $m' = 1/m$ that assumes the values $0 < m' < 1$ for the oscillating case. The sn-function has the transformation property $\mathrm{sn}\left(\sqrt{m'}x\middle| 1/m'\right) = \sqrt{m'}\,\mathrm{sn}\left(x\middle| m'\right)$ that allows to rewrite $\cos\theta(s)$ as follows:

$$\cos\theta(s) = 2m'\mathrm{sn}^2\left(\frac{s}{\lambda}\middle| m'\right) - 1. \tag{C.37}$$

To get parametric plots we calculate again the X- and Y-coordinates, Eq. C.32. With $\sin\theta(s) = \sqrt{1 - \cos^2\theta(s)}$ we find

$$\begin{aligned}\sin\theta(s) &= 2\sqrt{m'}\mathrm{sn}\left(\frac{s}{\lambda}\middle| m'\right)\sqrt{1 - m'\mathrm{sn}^2\left(\frac{s}{\lambda}\middle| m'\right)} \\ &= 2\sqrt{m'}\mathrm{sn}\left(\frac{s}{\lambda}\middle| m'\right)\mathrm{dn}\left(\frac{s}{\lambda}\middle| m'\right).\end{aligned} \tag{C.38}$$

Integrating this leads to

$$x(s) = 2\sqrt{m'}\lambda\left(1 - \mathrm{cn}\left(\frac{s}{\lambda}\middle| m'\right)\right). \tag{C.39}$$

The integration of $\cos\theta$ goes along similar lines as Eq. C.35:

$$y(s) = s - 2\lambda E\left(\mathrm{am}\left(\frac{s}{\lambda}\middle| m'\right)\middle| m'\right). \tag{C.40}$$

Appendix D

Fourier Series

Consider a complex-valued function f on the interval $[0, a]$ or, equivalently, a periodic function f of periodicity a. Let us try to approximate f by functions of the form

$$g_N(t) = \sum_{n=-N}^{+N} a_n e^{2\pi i n t/a}. \tag{D.1}$$

We ask ourselves: How should the coefficients a_n be chosen such that $f(t)$ is approximated by $g_N(t)$ as well as possible? More specifically, let us find the a_n-values $(-N \leq n \leq N)$ such that the mean-squared deviation Δ_N between f and g_N, namely

$$\Delta_N = \int_0^a |f(t) - g_N(t)|^2 \, dt, \tag{D.2}$$

is minimal. To solve this task we introduce the following notation:

$$\langle f, g \rangle = \int_0^a f^*(t)\, g(t)\, dt \tag{D.3}$$

where the star indicates the complex conjugate of a complex number (e.g., $z = a + ib$, $z^* = a - ib$). One has $\langle f, g \rangle = \langle g, f \rangle^*$, $\langle f, \alpha_1 g_1 + \alpha_2 g_2 \rangle = \alpha_1 \langle f, g_1 \rangle + \alpha_2 \langle f, g_2 \rangle$ for any complex numbers α_1 and α_2, and $\langle f, f \rangle > 0$ for any continuous f except $f \equiv 0$. Mathematically speaking $\langle ., . \rangle$ is an inner product on the vector space of continuous complex-valued functions on the interval $[0, a]$. The functions

$$\varphi_n(t) = \frac{1}{\sqrt{a}} e^{2\pi i n t/a} \tag{D.4}$$

fulfill the condition

$$\langle \varphi_n, \varphi_m \rangle = \delta_{nm} \tag{D.5}$$

i.e., they form an orthonormal system.

We rewrite now the problem of minimizing Eq. D.2 as follows. What are the values of the coefficients b_n with $-N \leq n \leq N$ such that

$$\Delta_N = \left\langle f - \sum_{n=-N}^{+N} b_n \varphi_n,\ f - \sum_{n=-N}^{+N} b_n \varphi_n \right\rangle \tag{D.6}$$

is as small as possible? Using two of the properties of the inner product we find:

$$\Delta_N = \langle f,\ f \rangle - \sum_{n=-N}^{+N} \left(b_n^* \langle \varphi_n,\ f \rangle + b_n \langle f,\ \varphi_n \rangle \right) + \sum_{n,m=-N}^{+N} b_m^* b_n \langle \varphi_m,\ \varphi_n \rangle . \tag{D.7}$$

Introducing $c_n = \langle \varphi_n,\ f \rangle$ and using the orthonormality of the φ_i's, this can be rewritten as

$$\Delta_N = \langle f,\ f \rangle - \sum_{n=-N}^{+N} \left(b_n^* c_n + b_n c_n^* - b_n^* b_n - c_n^* c_n + c_n^* c_n \right) \tag{D.8}$$

where we added and subtracted $c_n^* c_n$. This leads to

$$\Delta_N = \langle f,\ f \rangle - \sum_{n=-N}^{+N} |c_n|^2 + \sum_{n=-N}^{+N} |b_n - c_n|^2 . \tag{D.9}$$

From this expression we can directly see that Δ_n is minimal if one chooses $b_n = c_n \equiv \langle \varphi_n,\ f \rangle$. Note that the c_n's are independent of N. That means if you choose a higher number of terms to approximate f, you do not have to adjust the coefficients b_n—just as is the case when one approximates a function by a Taylor series.

The infinite series

$$\sum_{n=-\infty}^{+\infty} \langle \varphi_n,\ f \rangle \varphi_n(t) = \frac{1}{\sqrt{a}} \sum_{n=-\infty}^{+\infty} c_n e^{2\pi \mathrm{i} n t/a} \tag{D.10}$$

is called the Fourier series of the function f. It has been shown that the mean-squared deviation vanishes in the limit $N \to \infty$. That is even true for functions with a finite number of jumps where the Fourier series converges at any given point outside the jump discontinuities. The coefficients c_n are called Fourier coefficients.

The set $\{\varphi_n \,|n = 0, \pm 1, \pm 2, \dots\}$ represents a complete orthonormal system of functions. The Fourier series

$$f(t) = \sum_{n=-\infty}^{+\infty} \langle \varphi_n,\, f\rangle\, \varphi_n(t) \tag{D.11}$$

is analogous to the representation of a vector by an orthonormal basis. Especially, one has

$$\langle f,\, f\rangle = \int_0^a f^*(t)\, f(t)\, dt = \sum_{n=-\infty}^{+\infty} c_n^* c_n. \tag{D.12}$$

Another complete orthonormal system is given by the set of functions

$$\frac{1}{\sqrt{a}}, \quad \sqrt{\frac{2}{a}} \cos\left(\frac{2\pi nt}{a}\right), \quad \sqrt{\frac{2}{a}} \sin\left(\frac{2\pi nt}{a}\right) \tag{D.13}$$

with $n = 1, 2, \dots$. These functions are simply the normalized real and imaginary parts of the function $\varphi_n(t)$, Eq. D.4. The Fourier series, Eq. D.11, takes in this new system the form

$$f(t) = \frac{1}{\sqrt{a}} \sum_{n=0}^{\infty} \left[a_n \cos\left(\frac{2\pi nt}{a}\right) + b_n \sin\left(\frac{2\pi nt}{a}\right)\right] \tag{D.14}$$

with

$$a_0 = c_0 = \frac{1}{\sqrt{a}} \int_0^a f(t)\, dt, \tag{D.15}$$

$$a_n = (c_n + c_{-n}) = \frac{2}{\sqrt{a}} \int_0^a f(t) \cos\left(\frac{2\pi nt}{a}\right) dt \tag{D.16}$$

for $n > 0$, and

$$b_n = \mathrm{i}\,(c_n - c_{-n}) = \frac{2}{\sqrt{a}} \int_0^a f(t) \sin\left(\frac{2\pi nt}{a}\right) dt \tag{D.17}$$

for $n > 0$.

We mention two further complete orthonormal sets on $[0, a]$ from which Fourier series can be built. One is the set $\sqrt{2/a}\sin(\pi nt/a)$ with $n = 1, 2, \dots$ and the other is given by

$$\frac{1}{\sqrt{a}}, \quad \sqrt{\frac{2}{a}} \cos\left(\frac{\pi nt}{a}\right). \tag{D.18}$$

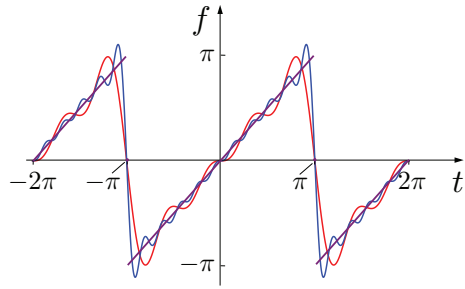

Figure D.1 Two approximations to the function $f(t) = t$ (shown in purple) on the interval $-\pi < t \leq \pi$. The red curve corresponds to the first 4 terms of its Fourier series, Eq. D.21, the blue curve to the first 10 terms.

with $n = 1, 2, \ldots$. Those systems are obtained by attributing to each function on $[0, a]$ an antisymmetric or symmetric function on $[-a, a]$, respectively. Fourier series of (anti)symmetric functions on $[-a, a]$ contain obviously only (anti)symmetric trigonometric terms.

We give now one example, namely $f(t) = t$ for $-\pi < t \leq \pi$, see Fig. D.1. In that case one finds

$$c_n = \frac{1}{\sqrt{2\pi}} \int_{-\pi}^{+\pi} te^{-\mathrm{i}nt} dt = \sqrt{2\pi}\, \mathrm{i} \frac{(-1)^n}{n} \tag{D.19}$$

for $n \neq 0$ and $c_0 = 0$. Hence

$$f(t) = \mathrm{i} \sum_{n=1}^{\infty} \frac{(-1)^n}{n} \left(e^{\mathrm{i}nt} - e^{-\mathrm{i}nt}\right) \tag{D.20}$$

and thus

$$t = 2 \sum_{n=1}^{\infty} (-1)^{n+1} \frac{\sin nt}{n} \tag{D.21}$$

for $-\pi < t < \pi$.

Appendix E

The Pre-Averaging Approximation

Free Gaussian chain: The idea is to replace $\mathbf{H}_{nm}$ by its average $\langle \mathbf{H}_{nm} \rangle_{\text{eq}}$ over the equilibrium distribution of the Gaussian chain [Doi and Edwards (1986)]. Since the orientation of $\mathbf{R}_{nm}$ is independent of its length, $\langle \mathbf{H}_{nm} \rangle_{\text{eq}}$ is of the form

$$\langle \mathbf{H}_{nm} \rangle_{\text{eq}} = \frac{1}{8\pi\eta} \left\langle \frac{1}{|\mathbf{R}_{nm}|} \right\rangle_{\text{eq}} \left\langle \mathbf{I} + \hat{\mathbf{R}}_{nm} \hat{\mathbf{R}}_{nm} \right\rangle_{\text{eq}} \tag{E.1}$$

that with $\left\langle \hat{\mathbf{R}}_{nm} \hat{\mathbf{R}}_{nm} \right\rangle_{\text{eq}} = \mathbf{I}/3$ simplifies to

$$\langle \mathbf{H}_{nm} \rangle_{\text{eq}} = \frac{\mathbf{I}}{6\pi\eta} \left\langle \frac{1}{|\mathbf{R}_{nm}|} \right\rangle_{\text{eq}}. \tag{E.2}$$

Internal monomer distances are Gaussian distributed with variances $b^2 |n-m|$, Eq. 5.102, allowing to calculate $\langle \mathbf{H}_{nm} \rangle_{\text{eq}}$ exactly

$$\begin{aligned} \langle \mathbf{H}_{nm} \rangle_{\text{eq}} &= \left(\frac{3}{2\pi b^2 |n-m|} \right)^{3/2} \int_0^\infty e^{-\frac{3r^2}{2b^2|n-m|}} \frac{\mathbf{I}}{6\pi\eta r} 4\pi r^2 dr \\ &= \frac{\mathbf{I}}{\sqrt{6\pi^3 |n-m|}\, \eta b} = h(n-m)\, \mathbf{I}. \end{aligned} \tag{E.3}$$

Replacing now in Eq. 5.134 $\mathbf{H}_{nm}$ by its average, $\langle \mathbf{H}_{nm} \rangle_{\text{eq}}$, leads to

$$\frac{\partial \mathbf{R}_n(t)}{\partial t} = \int_0^N h(n-m) \left(K \frac{\partial^2 \mathbf{R}_m(t)}{\partial m^2} + \mathbf{L}(m,t) \right) dm. \tag{E.4}$$

Through the pre-averaging approximation we arrived at a linear set of equations for the $\mathbf{R}_m$'s that, as in the Rouse model, decouples in

the X-, Y- and Z-components. The motion of monomers, however, is strongly coupled since $h(n-m) \sim |n-m|^{-1/2}$.

We analyze Eq. E.4 in terms of the Rouse normal coordinates, Eq. 5.110. To do so we first apply the transformation, Eq. 5.110, on both sides of Eq. E.4. By doing so one goes on the left-hand side from $\mathbf{R}_n(t)$ to $\mathbf{R}(p,t)$ and on the right-hand side from a function with two variables $h(n,m) = h(n-m)$ to a function with one Fourier transformed variable $h_p(m)$. As a second step one replaces the functions in m, $h_p(m)$, $\mathbf{R}_m(t)$ and $\mathbf{L}(m,t)$ by their Fourier series (as in Eq. 5.109) and performs the integration $\int_0^N dm$. One arrives then at

$$\frac{\partial \mathbf{R}(p,t)}{\partial t} = \sum_q h_{pq}\left(-K_q \mathbf{R}(q,t) + \tilde{\mathbf{L}}(q,t)\right). \tag{E.5}$$

Here K_q is defined by Eq. 5.113 and

$$h_{pq} = \frac{1}{N^2}\int_0^N dn \int_0^N dm \cos\left(\frac{p\pi n}{N}\right)\cos\left(\frac{q\pi m}{N}\right) h(n-m). \tag{E.6}$$

For $p, q > 0$ this can be rewritten as follows

$$\begin{aligned} h_{pq} &= \frac{1}{N^2}\int_0^N dn \int_{-n}^{N-n} dm \cos\left(\frac{p\pi n}{N}\right)\cos\left(\frac{q\pi (n+m)}{N}\right) h(m) \\ &= \frac{1}{N^2}\int_0^N dn \cos\left(\frac{p\pi n}{N}\right)\left[\cos\left(\frac{q\pi n}{N}\right)\int_{-n}^{N-n}\cos\left(\frac{q\pi m}{N}\right) h(m)\, dm \right. \\ &\quad \left. - \sin\left(\frac{q\pi n}{N}\right)\int_{-n}^{N-n}\sin\left(\frac{q\pi m}{N}\right) h(m)\, dm\right]. \end{aligned} \tag{E.7}$$

For large q the two $\int_{-n}^{N-n}$-integrals converge quickly to

$$\int_{-\infty}^{\infty}\cos\left(\frac{q\pi m}{N}\right) h(m)\, dm = \frac{1}{\eta b}\sqrt{\frac{N}{3\pi^3 q}} \tag{E.8}$$

and

$$\int_{-\infty}^{\infty}\sin\left(\frac{q\pi m}{N}\right) h(m)\, dm = 0. \tag{E.9}$$

Replacing the $\int_{-n}^{N-n}$-integrals in Eq. E.7 by these asymptotic values one obtains

$$h_{pq} \approx \frac{1}{\eta b}\sqrt{\frac{N}{3\pi^3 q}}\frac{1}{N^2}\int_0^N \cos\left(\frac{p\pi n}{N}\right)\cos\left(\frac{q\pi n}{N}\right)dn = \frac{\delta_{pq}}{\sqrt{12\pi^3 q N}\,\eta b}. \tag{E.10}$$

This relation also allows to estimate $h_{0q} \approx 0$ for $q > 1$. Finally h_{00} follows directly from Eq. E.6:

$$h_{00} = \frac{1}{N^2}\int_0^N dn \int_0^N dm\, h(n-m) = \frac{8}{3}\frac{1}{\sqrt{6\pi^3 N}\eta b}. \tag{E.11}$$

These equations indicate that h_{qp} is nearly diagonal. The Rouse modes are effectively decoupled – despite the presence of hydrodynamic interactions that make Eq. 5.134 nonlinear. The equation for the p-th mode has thus the same structure as the one for the Rouse model, Eq. 5.111:

$$\zeta_p \frac{\partial \mathbf{R}(p,t)}{\partial t} = -K_p \mathbf{R}(p,t) + \tilde{\mathbf{L}}(p,t). \tag{E.12}$$

with $\zeta_p = 1/h_{pp}$. The only difference to the Rouse model lies in the functional form of the ζ_p's. In the Zimm model we find

$$\zeta_0 = \frac{3}{8}\eta b\sqrt{6\pi^3 N},\ \ \zeta_p = \eta b\sqrt{12\pi^3 N p} \tag{E.13}$$

for $p = 1, 2, \ldots$ whereas ζ_p is constant for the Rouse model, Eq. 5.112.

Gaussian chain under tension: We estimate the mean distances between pairs of monomers in equilibrium using the Pincus blob argument, see Fig. 3.10. According to this argument one has a characteristic subchain monomer number $g_P = (k_B T/bf)^2$ such that monomers n and m belong to the same blob if $|n-m| < g_P$ and to different blobs if $|n-m| > g_P$. Hence

$$\langle |\mathbf{R}_{nm}| \rangle_{\text{eq}} \approx \begin{cases} b\,|n-m|^{1/2} & \text{for } |n-m| < g_P \\ \frac{b^2 f |n-m|}{k_B T} & \text{for } |n-m| > g_P. \end{cases} \tag{E.14}$$

Furthermore the average value of the tensor $\mathbf{I} + \hat{\mathbf{R}}_{nm}\hat{\mathbf{R}}_{nm}$ is $(4/3)\,\mathbf{I}$ for $|n=m| < g_P$ (isotropic case; see also the force free case above) and $\mathbf{I} + \mathbf{e}_y\mathbf{e}_y$ with $\mathbf{e}_y$ denoting the unit vector in the Y-direction,

the direction of the force. Neglecting that anisotropy (and numerical factors), i.e., setting $\left\langle \mathbf{I} + \hat{\mathbf{R}}_{nm}\hat{\mathbf{R}}_{nm} \right\rangle_{\mathrm{eq}} \approx \mathbf{I}$ we obtain

$$\langle \mathbf{H}_{nm} \rangle_{\mathrm{eq}} = h\,(n-m)\,\mathbf{I} \approx \begin{cases} \frac{\mathbf{I}}{\eta b |n-m|^{1/2}} & \text{for } |n-m| < g_P \\ \frac{\mathbf{I}}{\eta \left(b^2 f / k_{\mathrm{B}} T\right) |n-m|} & \text{for } |n-m| > g_P. \end{cases} \tag{E.15}$$

After the pre-averaging we arrive thus again at Eq. E.4 yet with a different function $h\,(n-m)$. In terms of the Rouse normal coordinates this leads to Eq. E.5 with K_q given by Eq. 5.113 and h_{pq} by Eq. E.6. h_{pq} for $p, q > 0$ can be calculated along a similar line as above in Eqs. E.7 to E.10. Here, however, Eq. E.8 needs to be replaced by

$$\int_{-\infty}^{\infty} \cos\left(\frac{q\pi m}{N}\right) h\,(m)\,dm \approx \frac{1}{\eta b}\left(\sqrt{\frac{N}{q}} \int_{0}^{\frac{q\pi g_P}{N}} \frac{\cos x}{x^{1/2}} dx + \frac{k_{\mathrm{B}} T}{bf} \int_{\frac{q\pi g_P}{N}}^{\infty} \frac{\cos x}{x} dx\right) \tag{E.16}$$

leading to

$$h_{pq} \approx \frac{1}{\eta b N}\left(\sqrt{\frac{N}{q}} \int_{0}^{\frac{q\pi g_P}{N}} \frac{\cos x}{x^{1/2}} dx + \frac{k_{\mathrm{B}} T}{bf} \int_{\frac{q\pi g_P}{N}}^{\infty} \frac{\cos x}{x} dx\right) \delta_{pq}. \tag{E.17}$$

From the asymptotic behavior of the integrals, the first being a Fresnel integral and the second the Cosine integral, one finds the asymptotic behavior of h_{pq}:

$$h_{pq} \approx \begin{cases} \frac{k_{\mathrm{B}} T}{\eta b^2 N f} \ln\left(\frac{N}{p\pi g_P}\right) \delta_{pq} & \text{for } p \ll \frac{N}{g_P} \\ \frac{1}{\eta b \sqrt{Np}}\, \delta_{pq} & \text{for } p \gg \frac{N}{g_P}. \end{cases} \tag{E.18}$$

The dynamics of the different Rouse modes are again given by Eq. E.12 with $\zeta_p = 1/h_{pp}$ now given by Eq. E.18. The behavior of short wavelength modes with large p, $p \gg N/g_P$, scale as in the case of a Zimm chain in the absence of a force, $\zeta_p \propto \eta b \sqrt{Np}$, Eq. E.10. Remarkably, the behavior of large wavelength modes with $p \ll N/g_P$ is entirely different. Neglecting the logarithmic factor in

Eq. E.18 we find $\zeta_p \approx \eta b^2 N f / k_\mathrm{B} T$ that is independent of p. This suggests that the long wavelength modes behave effectively Rouse-like. In complete analogy to the Rouse model (see Eq. 5.119) we find relaxation times for those modes of the form

$$\tau_p = \frac{\zeta_p}{K_p} = \frac{\tilde{\tau}_\mathrm{R}}{p^2} \tag{E.19}$$

with the Rouse time $\tilde{\tau}_\mathrm{R}$ given by Eq. 5.139.

Appendix F

Interaction between two Equally Charged Plates at Zero Temperature

Here we derive the pressure between two equally charged plates at zero temperature, Eq. 7.66. We begin by rewriting the sum over l in Eq. 7.65:

$$I = l_{\mathrm{B}} \sum_l \frac{1}{\sqrt{|\mathbf{R}_l + \mathbf{c}|^2 + D^2}} = l_{\mathrm{B}} \int d^2 r \sum_l \frac{\delta(\mathbf{r} - \mathbf{R}_l)}{\sqrt{|\mathbf{r} + \mathbf{c}|^2 + D^2}}. \quad \text{(F.1)}$$

The XY-positions of the ions on one surface form a lattice given by the set of 2D vectors $\mathbf{R}_l$, whereas the ions on the other surface are shifted to the positions $\mathbf{R}_l + \mathbf{c}$. The integral introduced above is thus two dimensional. The sum over the delta-functions is a periodic function in two dimensions. Any such periodic function $f(\mathbf{r})$ can be written in the form of a plane wave expansion, a 2D version of the Fourier expansion introduced in Appendix D. Here

$$f(\mathbf{r}) = \sum_l \delta(\mathbf{r} - \mathbf{R}_l) = \sum_{\mathbf{k}} f_{\mathbf{k}} e^{i\mathbf{kr}} \quad \text{(F.2)}$$

where the summation goes over all vectors $\mathbf{k}$ of the reciprocal lattice that is defined further below. The $f_{\mathbf{k}}$ are the Fourier coefficients that are given by

$$f_{\mathbf{k}} = \sigma \int_C e^{-i\mathbf{kr}} f(\mathbf{r})\, d\mathbf{r} \quad \text{(F.3)}$$

with C denoting a primitive cell of the direct lattice, a minimum repeat unit containing one ion. Here $f_{\mathbf{k}} = \sigma$ and hence

$$I = l_{\mathrm{B}}\sigma \sum_{\mathbf{k}} \int \frac{e^{i\mathbf{kr}}}{\sqrt{|\mathbf{r}+\mathbf{c}|^2 + D^2}} d^2r = l_{\mathrm{B}}\sigma \sum_{\mathbf{k}} e^{-i\mathbf{kc}} \int \frac{e^{i\mathbf{kr}}}{\sqrt{r^2+D^2}} d^2r. \tag{F.4}$$

We exchanged here the order of summation and integration; substituting $\mathbf{r}+\mathbf{c}$ by $\mathbf{r}$ yields the phase factor $e^{-i\mathbf{kc}}$. Note that the term with $\mathbf{k} = \mathbf{0}$ in the summation corresponds exactly to the second term in Eq. 7.65. Hence we can write the dimensionless potential as

$$\Phi(D) = l_{\mathrm{B}}\sigma \sum_{\mathbf{k}\neq\mathbf{0}} e^{-i\mathbf{kc}} \int \frac{e^{i\mathbf{kr}}}{\sqrt{r^2+D^2}} d^2r. \tag{F.5}$$

Using Eq. 7.66 we calculate the pressure from the potential by differentiation:

$$\begin{aligned}\frac{\Pi(D)}{k_{\mathrm{B}}T} &= l_{\mathrm{B}}\sigma^2 D \sum_{\mathbf{k}\neq\mathbf{0}} e^{-i\mathbf{kc}} \int \frac{e^{i\mathbf{kr}}}{\left(r^2+D^2\right)^{3/2}} d^2r \\ &= l_{\mathrm{B}}\sigma^2 D \sum_{\mathbf{k}\neq\mathbf{0}} e^{-i\mathbf{kc}} \int_0^{2\pi} d\phi \int_0^{\infty} dr \frac{r e^{ikr\cos\phi}}{\left(r^2+D^2\right)^{3/2}}.\end{aligned}$$

We introduced here polar coordinates where ϕ denotes the angle between the respective $\mathbf{k}$-vector and $\mathbf{r}$. The double integral can be calculated analytically (first integrate over ϕ, then over r) and yields $(2\pi/D)\, e^{-kD}$ with $k = |\mathbf{k}|$. This leads to

$$\frac{\Pi(D)}{k_{\mathrm{B}}T} = 2\pi l_{\mathrm{B}}\sigma^2 \sum_{\mathbf{k}\neq\mathbf{0}} e^{-i\mathbf{kc}} e^{-kD}. \tag{F.6}$$

We have thus expressed the interaction between the two surfaces as an infinite sum of exponentials. In the following we are interested in the leading terms of this sum for large distances. These will be the terms with the smallest value of k.

The ground state of a single plane is given by counterions that form a triangular Wigner crystal. We expect that each surface with its counterions still remains in this triangular ground state as long as D is much larger than the spacing between counterions within their planes. More specifically, the positions of the counterions in one lattice are given by $n_1\mathbf{a}_1 + n_2\mathbf{a}_2$ with $n_i = 0, \pm1, \pm2, \ldots$, an

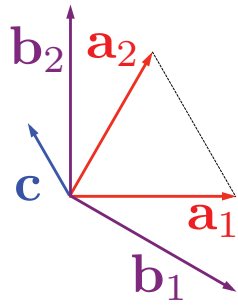

Figure F.1 Primitive vectors $\mathbf{a}_1$ and $\mathbf{a}_2$ that span the triangular lattice. Also indicated are the primitive vectors of the reciprocal lattice, $\mathbf{b}_1$ and $\mathbf{b}_2$, and the shiftvector $\mathbf{c}$ for maximal attraction between the two surfaces.

example of a so-called Bravais lattice. The vectors $\mathbf{a}_i$ that span the lattice, the so-called primitive vectors, are given by

$$\mathbf{a}_1 = a\mathbf{e}_x, \;\; \mathbf{a}_2 = \frac{a}{2}\mathbf{e}_x + \frac{\sqrt{3}a}{2}\mathbf{e}_y \tag{F.7}$$

and are indicated in Fig. F.1. The lattice spacing a has to be chosen such to match the charge density σ, leading to $a = 2/\left(3^{1/4}\sigma^{1/2}\right)$. The reciprocal lattice, the set of all vectors $\mathbf{k}$ for which $e^{i\mathbf{kR}} = 1$ for all $\mathbf{R}$ in the Bravais lattice, is given by $\mathbf{k} = k_1\mathbf{b}_1 + k_2\mathbf{b}_2$, $k_i = 0, \pm 1, \pm 2, \ldots$, with

$$\mathbf{b}_1 = \frac{2\pi}{a}\left(\mathbf{e}_x - \frac{1}{\sqrt{3}}\mathbf{e}_y\right), \;\; \mathbf{b}_2 = \frac{4\pi}{\sqrt{3}a}\mathbf{e}_y. \tag{F.8}$$

The primitive vectors of the reciprocal lattice fulfill $\mathbf{b}_i\mathbf{a}_j = 2\pi\delta_{ij}$, see also Fig. F.1. For large distances the leading terms in Eq. F.6 are the ones with the smallest value of k, namely $(k_1, k_2) = (\pm 1, 0)$ and $(k_1, k_2) = (0, \pm 1)$. For distances D with $D \gg a$ all higher order terms are negligible and, to a very good approximation, the large distance pressure is given by

$$\frac{\Pi(D)}{k_B T} \approx 4\pi\sigma^2 l_B \left(\cos(\mathbf{b}_1\mathbf{c}) + \cos(\mathbf{b}_2\mathbf{c})\right) e^{-\frac{4\pi}{\sqrt{3}a}D}. \tag{F.9}$$

For a vanishing length of $\mathbf{c}$ counterions of one surface are just on top of counterions of the other surface so that the two surfaces repel each other. One finds then $\cos(\mathbf{b}_1\mathbf{c}) + \cos(\mathbf{b}_2\mathbf{c}) = 2$ leading to maximal repulsion. If we, however, allow one of the plates with its counterions to move in the XY-plane relative to the other at a fixed

value of D, the system can lower its energy. It reaches the ground state when $\cos(\mathbf{b}_1\mathbf{c}) + \cos(\mathbf{b}_2\mathbf{c}) = -2$. This can be achieved by choosing e.g., the shift c such that $\mathbf{b}_1\mathbf{c} = -\pi$ and $\mathbf{b}_2\mathbf{c} = \pi$. This is achieved for

$$\mathbf{c} = -\frac{a}{4}\mathbf{e}_x + \frac{\sqrt{3}a}{4}\mathbf{e}_y, \tag{F.10}$$

as shown in Figs. 7.12 and F.1. We find then Eq. 7.66 from Eq. F.9.

Appendix G

Geometries of Chromatin Fiber Models

Two-angle model: For any given set of angles (θ, ϕ) in the two-angle model there is a helix, the master solenoid, so that all the successive vertices (see Fig. 8.33(b))—called monomers in the following—lie along that helical path. There are actually many such solutions, but we are interested in the one with the largest pitch angle ψ, see Fig. G.1. We parametrize the solenoid as follows

$$\mathbf{r}(s) = \begin{pmatrix} R\cos(\alpha s/R) \\ R\sin(\alpha s/R) \\ s \end{pmatrix}. \tag{G.1}$$

R denotes the radius of the solenoid and α is related to the pitch ψ by

$$\alpha = \cot\psi \tag{G.2}$$

since $\dot{\mathbf{r}}(0) = (0, \alpha, 1)$.

Assume now an infinite fiber of monomers with a given pair of angles (θ, ϕ). The monomers are located at the positions $\mathbf{R}_0, \mathbf{R}_{\pm1}, \mathbf{R}_{\pm2}, \ldots$. The axis of the fiber coincides with the Z-axis. Put the monomer labeled $i = 0$ at $s = 0$ so that $\mathbf{R}_0 = \mathbf{r}(0) = (R, 0, 0)$. The next monomer, $i = 1$, is at a position $\mathbf{R}_1 = \mathbf{r}(s_0)$ and the next nearest monomer at $\mathbf{R}_2 = \mathbf{r}(2s_0)$. Finally, the position of monomer $i = -1$ is given by $\mathbf{R}_{-1} = \mathbf{r}(-s_0)$.

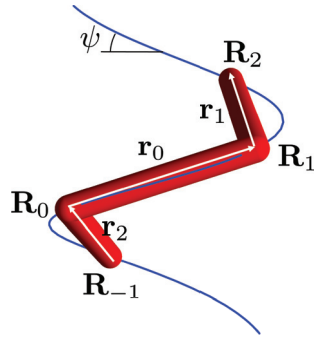

Figure G.1 The master solenoid (blue) and the linker DNA backbone (red) of the two-angle fiber.

Now let us calculate the bond vectors between these monomers, see Fig. G.1. Monomer $i = 1$ is connected to monomer $i = 0$ via

$$\mathbf{r}_0 = \mathbf{R}_1 - \mathbf{R}_0 = \begin{pmatrix} R\cos(\alpha s_0/R) - R \\ R\sin(\alpha s_0/R) \\ s_0 \end{pmatrix}. \tag{G.3}$$

The vector between monomer $i = 2$ and $i = 1$ is given by

$$\mathbf{r}_1 = \mathbf{R}_2 - \mathbf{R}_1 = \begin{pmatrix} R\cos(2\alpha s_0/R) - R\cos(\alpha s_0/R) \\ R\sin(2\alpha s_0/R) - R\sin(\alpha s_0/R) \\ s_0 \end{pmatrix} \tag{G.4}$$

and that between monomer $i = 0$ and $i = -1$ by

$$\mathbf{r}_2 = \mathbf{R}_0 - \mathbf{R}_{-1} = \begin{pmatrix} R - R\cos(\alpha s_0/R) \\ R\sin(\alpha s_0/R) \\ s_0 \end{pmatrix}. \tag{G.5}$$

s_0 follows from the condition of fixed linker length, i.e., $|\mathbf{r}_0| = b$. This leads to the relation

$$b^2 = 2R^2\left(1 - \cos(\alpha s_0/R)\right) + s_0^2. \tag{G.6}$$

We determine θ from $\cos\theta = \mathbf{r}_0 \cdot \mathbf{r}_2 / r_0^2$, which leads to

$$\cos\theta = \frac{2R^2\cos(\alpha s_0/R)\left(1 - \cos(\alpha s_0/R)\right) + s_0^2}{2R^2\left(1 - \cos(\alpha s_0/R)\right) + s_0^2}. \tag{G.7}$$

Finally, ϕ is the angle between normal vectors of the planes that are defined by monomers 0 and 1, i.e., $\cos\phi = \mathbf{n}_1 \cdot \mathbf{n}_2$. We obtain $\mathbf{n}_1$ and

$\mathbf{n}_2$ from $\mathbf{n}_1 = \mathbf{r}_0 \times \mathbf{r}_1/|\mathbf{r}_0 \times \mathbf{r}_1|$ and $\mathbf{n}_2 = \mathbf{r}_2 \times \mathbf{r}_0/|\mathbf{r}_2 \times \mathbf{r}_0|$. After some algebra we arrive at

$$\cos\phi = \frac{s_0^2 \cos(\alpha s_0/R) + R^2 \sin^2(\alpha s_0/R)}{s_0^2 + R^2 \sin^2(\alpha s_0/R)}. \tag{G.8}$$

Equations G.6–G.8 relate α (or ψ), R and s_0 of the master solenoid to θ, ϕ and b.

Solenoid-type models: The geometry of the two-angle model and that of solenoid-type models have in common that some part of the fiber forms a helix. For the two-angle model the helix is made of the linker DNA, Fig. G.1, for the solenoid-type models one has one or several helices formed by stacks of nucleosomes. This allows us to use the geometrical relations of the two-angle model to describe solenoid-type models. R from Eq. G.1 is now given by $(D_{\text{fiber}} - D_{\text{nucl}})/2$. According to Fig. 8.38 for a fiber with N_{rib} stacks this quantity is given by

$$\pi\,(D_{\text{fiber}} - D_{\text{nucl}}) = N_{\text{rib}} \frac{D_{\text{nucl}}}{\sin\psi} \tag{G.9}$$

where ψ is again given related to α via Eq. G.2. Equation G.1 gives us explicitly the space curve of one of the stacks, the other stacks follow by adding a constant $2\pi k/N_{\text{rib}}$ to the arguments of the trigonometric functions with $k = 1, 2, \ldots, N_{\text{rib}} - 1$.

The linker length b of the two-angle model is now replaced by the nucleosomal height H_{nucl}. We need to determine the arc length of a helix segment that crosses through a nucleosome in a stack. We know that the length of the tangent vector of the space curve, Eq. G.1, is given by $|\dot{\mathbf{r}}(s)| = \sqrt{1+\alpha^2}$. That means when s goes from $s = 0$ to $s = s_0 = H_{\text{nucl}}/\sqrt{1+\alpha^2}$ the helix crosses approximately the nucleosome. This is an approximation because the helix is curved but the error is negligible as long as $H_{\text{nucl}} \ll D_{\text{fiber}}$ as always assumed in the following.

The splay angle is identical to the angle θ of the two angle model. Since θ and $\alpha s_0/R$ are always small here, we can Taylor expand all the cosine functions in Eq. G.7. This leads to

$$\theta \approx \frac{s_0\alpha^2}{R\sqrt{1+\alpha^2}} = \frac{2H_{\text{nucl}}}{D_{\text{fiber}} - D_{\text{nucl}}} \frac{\alpha^2}{1+\alpha^2} = \frac{2H_{\text{nucl}}}{D_{\text{fiber}} - D_{\text{nucl}}} \left(1 - \sin^2\psi\right) \tag{G.10}$$

Replacing $\sin\psi$ by using Eq. G.9 we find Eq. 8.108.

References

Alberts, B., Johnson, A., Lewis, J., Raff, M., Roberts, K. and Walter, P. (2008). *Molecular Biology of the Cell*, 5th edn. (Garland Science, New York).

Alexander, S., Chaikin, P. M., Grant, P., Morales, G. J. and Pincus, P. (1984). Charge renormalization, osmotic pressure, and bulk modulus of colloidal crystals: theory, *J. Chem. Phys.* **80**, pp. 5776–5781.

Becker, N. B. and Everaers, R. (2007). From rigid base pairs to semiflexible polymers: Coarse-graining DNA, *Phys. Rev. E* **76**, pp. 021923–1–17.

Bednar, J., Horowitz, R. A., Grigoryev, S. A., Carruthers, L. M., Hansen, J. C., Koster, A. J. and Woodcock, C. L. (1998). Nucleosomes, linker DNA, and linker histone form a unique structural motif that directs the higher-order folding and compaction of chromatin, *Proc. Natl. Acad. Sci. USA* **95**, pp. 14173–14178.

Ben-Haïm, E., Lesne, A. and Victor, J.-M. (2001). Chromatin: a tunable spring at work inside chromosomes, *Phys. Rev. E* **64**, pp. 051921–1–19.

Berg, O. G., Winter, R. B. and von Hippel, P. H. (1981). Diffusion-driven mechanisms of protein translocation on nuclei acids. 1. Model and theory, *Biochemistry* **20**, pp. 6929–6948.

Blossey, R. (2006). *Computational Biology: a Statistical Physics Perspective* (Chapman & Hill/CRC, Boca Raton).

Brower-Toland, B. D., Smith, C. L., Yeh, R. C., Lis, J. T., Peterson, C. L. and Wang, M. D. (2002). Mechanical disruption of individual nucleosomes reveals a reversible multistage release of DNA, *Proc. Natl. Acad. Sci. USA* **99**, pp. 1960–1965.

Bruinsma, R. F. (2002). Physics of protein-DNA interaction, *Physica A* **313**, pp. 211–237.

Bustamante, C., Marko, J. F., Siggia, E. D. and Smith, S. (1994). Entropic elasticity of λ-phage DNA, *Science* **265**, pp. 1599–1600.

Calladine, C. R., Drew, H. R., Luisi, B. F. and Travers, A. A. (2004). *Understanding DNA: the Molecule and how it works*, 3rd edn. (Elsevier, Amsterdam).

Chan, H. S. and Dill, K. A. (1989). Compact polymers, *Macromolecules* **22**, pp. 4559–4573.

Chen, F. E., Huang, D.-B., Chen, Y.-Q. and Ghosh, G. (1998). Chrystal structure of p50/p65 heterodimer of transcription factor NF-κB bound to DNA, *Nature* **391**, pp. 410–413.

Cotton, J. P., Decker, D., Benoit, H., Farnoux, B., Higgins, J., Jannink, G., Ober, R., Picot, C. and des Cloizeaux, J. (1974). Conformation of polymer chain in the bulk, *Macromolecules* **7**, pp. 863–872.

Cui, Y. and Bustamante, C. (2000). Pulling a single chromatin fiber reveals the forces that maintain its higher-order structure, *Proc. Natl. Acad. Sci. USA* **97**, pp. 127–132.

Daban, J.-R. and Bermúdez, A. (1998). Interdigitated solenoid model for compact chromatin fibers, *Biochemistry* **37**, pp. 4299–4304.

de Gennes, P.-G. (1979). *Scaling Concepts in Polymer Physics* (Cornell University Press, Ithaca).

deHaseth, P. L., Lohman, T. M. and Record, M. T. (1977). Nonspecific interaction of *lac* repressor with DNA: an association reaction driven by counterion release, *Biochemistry* **16**, pp. 4783–4790.

Depken, M., Parrondo, J. M. R. and Grill, S. W. (2013). Intermittent transcription dynamics for the rapid production of long transcripts of high fidelity, *Cell Reports*, http://dx.doi.org/10.1016/j.celrep.2013.09.007

Depken, M. and Schiessel, H. (2009). Nucleosome shape dictates chromatin fiber structure, *Biophys. J.* **96**, pp. 777–784.

Diesinger, P. M. and Heermann, D. W. (2008). The influence of the cylindrical shape of the nucleosomes and H1 defects on properties of chromatin, *Biophys. J.* **94**, pp. 4165–4172.

Dill, K. A. and Chan, H. S. (1997). From Levinthal to pathways to funnels, *Nature Struct. Biol.* **4**, pp. 10–19.

Doi, M. and Edwards, S. F. (1986). *The Theory of Polymer Dynamics* (Oxford University Press, New York).

Dorigo, B., Schalch, T., Kulangara, A., Duda, S., Schroeder, R. R. and Richmond, T. J. (2004). Nucleosome arrays reveal the two-start organization of the chromatin fiber, *Science* **306**, pp. 1571–1573.

Dubochet, J. and Noll, M. (1978). Nucleosome arcs and helices, *Science* **202**, pp. 280–286.

Elf, J., Li, G.-W. and Xie, X. S. (2007). Probing transcription factor dynamics at the single-molecule level in a living cell, *Science* **316**, pp. 1191–1194.

Eltsov, M., MacLellan, K. M., Maeshima, K., Frangakis, A. S. and Dubochet, J. (2008). Analysis of cryo-electron microscopy images does not support the existence of 30-nm chromatin fibers in mitotic chromosomes in situ, *Proc. Natl. Acad. Sci. USA* **105**, pp. 19732–19737.

Emanuel, M., Radja, N. H., Henriksson, A. and Schiessel, H. (2009). The physics behind the larger scale organization of DNA in eukaryotes, *Phys. Biol.* **6**, pp. 025008–1–11.

Evans, E. (1999). Looking inside molecular bonds at biological interfaces with dynamic force spectroscopy, *Biophys. Chem.* **82**, pp. 83–97.

Finch, J. T. and Klug, A. (1976). Solenoidal model for superstructure in chromatin, *Proc. Natl. Acad. Sci. USA* **73**, pp. 1897–1901.

Fisher, M. E. (1966). Effect of excluded volume on phase transitions in biopolymers, *J. Chem. Phys.* **45**, pp. 1469–1473.

Franklin, R. E. and Gosling, R. G. (1953). Molecular configuration in sodium thymonucleate, *Nature* **171**, pp. 740–741.

Geanacopoulos, M., Vasmatzis, G., Zhurkin, V. B. and Adhya, A. (2001). Gal repressosome contains an antiparallel DNA loop, *Nature Struct. Biol.* **8**, pp. 432–436.

Grosberg, A., Rabin, Y., Havlin, S. and Neer, A. (1993). Crumpled globule model of the three-dimensional structure of DNA, *Europhys. Lett.* **23**, pp. 373–378.

Hahnfeldt, P., Hearst, J. E., Brenner, D. J., Sachs, R. K. and Hlatky, L. R. (1993). Polymer models for interphase chromosomes, *Proc. Natl. Acad. Sci. USA* **90**, pp. 7854–7858.

Halford, S. E. and Marko, J. F. (2004). How do site-specific DNA-binding proteins find their targets? *Nucl. Acids Res.* **32**, pp. 3040–3052.

Halperin, A. and Zhulina, E. B. (1991). On the deformation behaviour of collapsed polymers, *Europhys. Lett.* **15**, pp. 417–421.

Hanke, A. and Metzler, R. (2003). Comment on "Why is the DNA denaturation transition first order?", *Phys. Rev. Lett.* **90**, pp. 159801–1.

Higgs, P. G. (2000). RNA secondary structure: physical and computational aspects, *Quart. Rev. Biophys.* **33**, pp. 199–253.

Hilbert, D. (1891). Ueber die stetige Abbildung einer Linie auf ein Flächenstück, *Mathematische Annalen* **38**, pp. 459–460.

Hopfield, J. J. (1974). Kinetic proofreading: a new mechanism for reducing errors in biosynthetic processes requiring high specificity, *Proc. Natl. Acad. Sci. USA* **71**, pp. 4135–4139.

Kafri, Y., Mukamel, D. and Peliti, L. (2002). Melting and unzipping of DNA, *Eur. Phys. J. B* **27**, pp. 135–146.

Kirchhoff, G. (1859). Ueber das Gleichgewicht und die Bewegung eines unendlich dünnen elastischen Stabes, *J. reine angew. Math.* **56**, pp. 285–313.

Kruithof, M., Chien, F.-T., Routh, A., Logie, C., Rhodes, D. and van Noort, J. (2009). Single-molecule force spectroscopy reveals a highly compliant helical folding for the 30-nm chromatin fiber, *Nature Struct. Mol. Biol.* **16**, pp. 534–540.

Kulić, I. M., Mohrbach, H., Thaokar, R. and Schiessel, H. (2007). Equation of state of looped DNA, *Phys. Rev. E* **75**, pp. 011913–1–23.

Kulić, I. M. and Schiessel, H. (2003a). Chromatin dynamics: nucleosomes go mobile through twist defects, *Phys. Rev. Lett.* **91**, pp. 148103–1–4.

Kulić, I. M. and Schiessel, H. (2003b). Nucleosomes repositioning via loop formation, *Biophys. J.* **84**, pp. 3197–3211.

Kulić, I. M. and Schiessel, H. (2004). DNA spools under tension, *Phys. Rev. Lett.* **92**, pp. 228101–1–4.

Lankaš, F., Gonzales, O., Heffler, L. M., Stoll, G., Moakher, M. and Maddocks, J. H. (2009). On the parametrization of rigid base and basepair models of DNA from molecular dynamics simulations, *Phys. Chem. Chem. Phys.* **11**, pp. 10565–10588.

Lanzani, G. and Schiessel, H. (2012). Out of register: how DNA determines the chromatin fiber geometry, *Europhys. Lett.* **97**, pp. 38002–1–6.

Lau, K. F. and Dill, K. A. (1989). A lattice statistical mechanics model for the conformational and sequence spaces of proteins, *Macromolecules* **22**, pp. 3986–3997.

Lau, K. F. and Dill, K. A. (1990). Theory for protein mutability and biogenesis, *Proc. Natl. Acad. Sci. USA* **87**, pp. 638–642.

Lia, G., Bensimon, D., Croquette, V., Allemand, J.-F., Dunlap, D., Lewis, D. E. A., Adhya, S. and Finzi, L. (2003). Supercoiling and denaturation in Gal repressor/heat unstable nucleoid protein (HU)-mediated DNA looping, *Proc. Natl. Acad. Sci. USA* **100**, pp. 11373–11377.

Lieberman-Aiden, E., van Berkum, N. L., Williams, L., Imakaev, M., Ragoczy, T., Telling, A., Amit, I., Lajoie, B. R., Sabo, P. J., Dorschner, M. O., Sandstrom, R., Bernstein, B., Bender, M. A., Groudine, M., Gnirke, A., Stamatoyannopoulos, J., Mirny, L. A., Lander, E. S. and Dekker, J. (2009). Comprehensive mapping of long-range interactions reveals folding principles of the human genome, *Science* **326**, pp. 289–293.

Lua, R., Borovinskiy, A. L. and Grosberg, A. Y. (2004). Fractal and statistical properties of large compact polymers: a computational study, *Polymer* **45**, pp. 717–731.

Luger, K., Mäder, A. W., Richmond, R. K., Sargent, D. F. and Richmond, T. J. (1997). Crystal structure of the nucleosome core particle at 2.8 Å resolution, *Nature* **389**, pp. 251–260.

Makarov, V., Dimitrov, S., Smirnov, V. and Pashev, I. (1985). A triple helix model for the structure of chromatin fiber, *FEBS Letters* **181**, pp. 357–361.

Mangenot, S., Leforestier, A., Durand, D. and Livolant, F. (2003). Phase diagram of nucleosome core particles, *J. Mol. Biol.* **333**, pp. 907–916.

Mangenot, S., Raspaud, E., Tribet, C., Belloni, L. and Livolant, F. (2002). Interactions between isolated nucleosome core particles: a tail-bridging effect? *Eur. Phys. J. E* **7**, pp. 221–231.

Marvin, D. A., Spencer, M., Wilkins, M. H. F. and Hamilton, L. D. (1958). A new configuration of deoxyribonucleic acid, *Nature* **182**, pp. 387–388.

Mateos-Langerak, J., Bohn, M., de Leeuw, W., Giromus, O., Manders, E. M. M., Verschure, P. J., Indemans, M. H. G., Gierman, H. J., Heermann, D. W., van Driel, R. and Goetze, S. (2009). Spatially confined folding of chromatin in the interphase nucleus, *Proc. Natl. Acad. Sci. USA* **106**, pp. 3812–3817.

Mihardja, S., Spakowitz, A. J., Zhang, Y. and Bustamante, C. (2006). Effect of force on mononucleosomal dynamics, *Proc. Natl. Acad. Sci. USA* **103**, pp. 15871–15876.

Moreira, A. G. and Netz, R. R. (2002). Simulations of counterions at charged plates, *Eur. Phys. J. E* **8**, pp. 33–58.

Münkel, C. and Langowski, J. (1998). Chromosome structure predicted by a polymer model, *Phys. Rev. E* **57**, pp. 5888–5896.

Neuman, K. C., Abbondanzieri, E. A., Landick, R., Gelles, J. and Block, S. M. (2003). Ubiquitous transcriptional pausing is independent of RNA polymerase backtracking, *Cell* **115**, pp. 437–447.

Odijk, T. (1995). Stiff chains and filaments under tension, *Macromolecules* **28**, pp. 7016–7018.

Olson, W. K., Srinivasan, A. R., Colasanti, A. V., Zheng, G. and Swigon, D. (2009). *DNA Biomechanics in: Handbook of Molecular Biophysics (ed.: H. G. Bohr)* (Wiley-VCH Verlag, Weinheim), pp. 359–382.

Onsager, L. (1949). The effects of shape on the interaction of colloidal particles, *Annals of the New York Academy of Sciences* **51**, pp. 627–659.

Pace, N. R. and Brown, J. W. (1995). Evolutionary perspective on the structure and function of ribonuclease P, a ribozyme, *J. Bacteriol.* **177**, pp. 1919–1928.

Pande, V. S., Joerg, C., Grosberg, A. Y. and Tanaka, T. (1994). Enumerations of the Hamiltonian walks on a cubic sublattice, *J. Phys. A: Math Gen.* **27**, pp. 6231–6236.

Pauling, L. and Corey, R. B. (1953). A proposed structure for the nucleic acids, *Proc. Natl. Acad. Sci. USA* **39**, pp. 84–97.

Pennings, S., Meersseman, G. and Bradbury, E. M. (1991). Mobility of positioned nucleosomes on 5 S rDNA, *J. Mol. Biol.* **220**, pp. 101–110.

Pincus, P. (1997). Dynamics of stretched polymer chains, *Macromolecules* **10**, pp. 210–213.

Polach, K. J. and Widom, J. (1995). Mechanism of protein access to specific DNA sequences in chromatin: a dynamic equilibrium model for gene regulation, *J. Mol. Biol.* **254**, pp. 130–149.

Poland, D. and Scheraga, H. A. (1966). Occurrence of a phase transition in nucleic acid models, *J. Chem. Phys.* **45**, pp. 1464–1469.

Prinsen, P. and Schiessel, H. (2010). Nucleosome stability and accessibility of its DNA to proteins, *Biochimie* **92**, pp. 1722–1728.

Riggs, A. D., Bourgeois, S. and Cohn, M. (1970). The *lac* repressor-operator interaction. III. Kinetic studies, *J. Mol. Biol.* **53**, pp. 401–417.

Robinson, P. J. J., Fairall, L., Huynh, V. A. T. and Rhodes, D. (2006). EM measurements define the dimensions of the 30-nm chromatin fiber: evidence for a compact, interdigitated structure, *Proc. Natl. Acad. Sci. USA* **103**, pp. 6506–6511.

Rosa, A. and Everaers, R. (2008). Structure and dynamics of interphase chromosomes, *PLoS Comp. Biol.* **4**, pp. e1000153–1–10.

Rouzina, I. and Bloomfield, V. A. (1996). Macroion attraction due to electrostatic correlation between screening counterions. 1. Mobile surface-adsorbed ions and diffuse ion cloud, *J. Phys. Chem.* **100**, pp. 9977–9989.

Schalch, T., Duda, S., Sargent, D. F. and Richmond, T. J. (2005). X-ray structure of a tetranucleosome and its implications for the chromatin fibre, *Nature* **436**, pp. 138–141.

Schiessel, H., Gelbart, W. M. and Bruinsma, R. (2001). DNA folding: structural and mechanical properties of the two-angle model for chromatin, *Biophys. J.* **80**, pp. 1940–1956.

Segal, E., Fondufe-Mittendorf, Y., Chen, L., Thåström, A., Field, Y., Moore, I. K., Wang, J.-P. Z. and Widom, J. (2006). A genomic code for nucleosome positioning, *Nature* **442**, pp. 772–778.

Shakhnovich, E. and Gutin, A. (1990). Enumeration of all compact conformations of copolymers with random sequence of links, *J. Chem. Phys.* **93**, pp. 5967–5971.

Smith, S. B., Finzi, L. and Bustamante, C. (1992). Direct mechanical measurements of the elasticity of single DNA molecules by using magnetic beads, *Science* **258**, pp. 1122–1126.

Sudhanshu, B., Mihardja, S., an, E. F. K., Mehraeen, S., Bustamante, C. and Spakowitz, A. J. (2011). Tension-dependent structural deformation alters single-molecule transition kinetics, *Proc. Natl. Acad. Sci. USA* **108**, pp. 1885–1890.

Syed, S. H., Goutte-Gattat, D., Becker, N., Meyer, S., Shukla, M. S., Hayes, J. J., Everaers, R., Angelov, D., Bednar, J. and Dimitrov, S. (2010). Single-base resolution mapping of H1-nucleosome interactions and 3D organization of the nucleosome, *Proc. Natl. Acad. Sci. USA* **107**, pp. 9620–9625.

Tolstorukov, M. Y., Colasanti, A. V., McCandlish, D. M., Olson, W. K. and Zhurkin, V. B. (2007). A novel roll-and-slide mechanism of DNA folding in chromatin: Implications for nucleosome positioning, *J. Mol. Biol.* **371**, pp. 725–738.

van Kampen, N. G. (1992). *Stochastic Processes in Physics and Chemistry* (Elsevier, Amsterdam).

Watson, J. D. (1968). *The Double Helix: a Personal Account of the Discovery of Structure of DNA* (Atheneum, New York).

Watson, J. D. and Crick, F. H. C. (1953). Molecular structure of nucleic acids – a structure for deoxyribose nucleic acid, *Nature* **171**, pp. 737–738.

Widom, J. (1992). A relationship between the helical twist of DNA and the ordered positioning of nucleosomes in all eukaryotic cells, *Proc. Natl. Acad. Sci. USA* **89**, pp. 1095–1099.

Winter, R. B., Berg, O. G. and von Hippel, P. H. (1981). Diffusion-driven mechanisms of protein translocation on nuclei acids. 3. The *Escherichia coli lac* repressor-operator interaction: Kinetic measurements and conclusions, *Biochemistry* **20**, pp. 6961–6977.

Woodcock, C. L., Grigoryev, S. A., Horowitz, R. A. and Whitaker, N. (1993). A chromatin folding model that incorporates linker variability generates fibers resembling the native structures, *Proc. Natl. Acad. Sci. USA* **90**, pp. 9021–9025.

Yeomans, J. M. (1992). *Statistical Mechanics of Phase Transitions* (Oxford University Press, New York).

Zimm, B. H. (1956). Dynamics of polymer molecules in dilute solution: viscoelasticity, flow birefringence and dielectric loss, *J. Chem. Phys.* **24**, pp. 269–278.

Index